JOURNAL OF AIRCRAFT
Vol. 46, No. 3, May–June 2009

Effect of Submerged Vortex Generators on Shock-Induced Separation in Transonic Flow

A. Zare Shahneh* and F. Motallebi†
Queen Mary, University of London, London, England E1 4NS, United Kingdom

DOI: 10.2514/1.37678

The effect of a tetrahedral vortex generator on the shock-induced boundary-layer separation has been investigated experimentally at a nominal Mach number of 1.4. The unit Reynolds number was 16×10^6 per meter. Two pairs of vortex generators with different heights have been used to control the shock/boundary-layer interaction. Each pair of vertex generators has been placed upstream of the shock location at a fixed distance of 130 mm, which corresponds to 18 times the boundary thickness. Measurements consist of mean boundary-layer profile and streamwise distribution of wall static pressure and Preston pressure. Experimental results suggests that both tetrahedral vortex generators influence and reduce the extent of boundary-layer separation as compared with the baseline configuration, in which no tetrahedral vortex generators were present. Experiments also revealed that the tetrahedral vortex generator with a height of 0.7δ did not produce further reduction in the extent of separation region as compared with the smaller tetrahedral vortex generator with a height of 0.4δ. The experiments confirm that a thicker vortex generator produces more displacement thickness at the expense of a thicker boundary layer and a lower Preston pressure. In both cases, the shape factor of the boundary layer at the location of shock wave showed a decrease of about 46% as compared with the baseline value.

Nomenclature

H	=	shape factor
h	=	vortex generator height, m
M	=	Mach number
P	=	pressure, Pa
P_s	=	wall static pressure, Pa
P_{stg}	=	settling chamber stagnation pressure, Pa
P_t	=	total pressure, Pa
U	=	streamwise velocity, m/s
U_δ	=	velocity at edge of boundary layer, m/s
X	=	streamwise coordinate direction
Y	=	vertical coordinate (normal to the wall)
Z	=	spanwise coordinate direction
δ	=	boundary-layer thickness, m
δ_R	=	boundary-layer thickness at reference point, m
δ^*	=	displacement thickness, m
δ^*_R	=	displacement thickness at reference point, m
θ	=	momentum thickness, m
θ_R	=	momentum thickness at reference point, m

I. Introduction

THE effect of the vortex generator on the attenuation of separation in the boundary-layer/shock-wave interaction is perhaps the most straightforward to understand. The interaction between a turbulent boundary layer and a shock wave is a feature frequently encountered in modern aerodynamics. When an aircraft approaches its critical speed, normal shock waves can form over its wings at transonic speeds. The interaction of the shock wave with the boundary-layer flow can result in flow separation, which in turn can reduce lift, increase drag, and, in some cases, cause buffeting. This phenomenon is associated with the formation of vortices and large energy losses at the interaction zone.

A number of investigations have been reported by several authors to introduce control methods to reduce or limit the side effects of flow separation due to its interaction with the shock waves. They include different forms of cavities, bumps, slots, and solid pieces as the vortex generator. A model of three-sided submerged channels was introduced by Wheeler [1] for the purpose of flow control. Different types of cavities have been proposed for the turbine nozzle of an aircraft engine [2–5]. Bur and Corbel [6] investigated a bump system and compared it with a suction system at ONERA. In another attempt, three slots were fitted above a cavity depth of 38 mm in the floor of the square wind-tunnel working section for flow control [7]. The preceding controllers were capable of producing vortices as a way of energizing the boundary-layer flow.

A vortex generator achieves boundary-layer control only at the penalty of possible considerable drag. A sub-boundary vortex generator (SBVG) produces vortices that travel downstream along the surface, causing flow mixing between the inner layers of the boundary layer. Although these SBVG will produce extra drag as compared with a clean surface, their drag penalty is much less than with vortex generators (VGs) which usually have a height of about the boundary-layer thickness or even more. In Wheeler's [8] work, the SBVGs submerged to about 60% of the local boundary-layer thickness and, positioned at the 22% of the chord, reduced the drag of an LA2573 Liebeck low-Reynolds-number airfoil. Vane-type vortex generators are the most common type of vortex generators and are small plates normal to the surface at a specific degree of angle of attack. The investigation on vane type that was carried out at NACA in 1950 [9] and then with a rectangular form of vane type [10,11] showed that this type of SBVG could prevent the boundary-layer separation. A trapezoid shape was compared with a delta-shaped vane-type SBVGs in the NASA Langley Research Center's low-turbulence wind tunnel. These SBVGs were mounted on the flap of an airfoil [12]. The effect of a common vane-type vortex generator was compared with the Wheeler type at NASA to verify the capabilities of different models for flow control [13,14].

To investigate the fundamental behavior of a SBVG, a group of researchers at Defence Evaluation and Research Agency (DERA) conducted a series of experiments in their boundary-layer tunnel [15], a three-component laser Doppler anemometry was used for the velocity measurement. The tunnel was of an open-return design with a long working section (1.2 m width by a nominal 0.3 m height). The

Received 22 March 2008; revision received 31 March 2009; accepted for publication 19 December 2008.

*School of Engineering and Material Sciences, Mile End Road; a.shahneh@qmul.ac.uk.

†School of Engineering and Material Sciences, Mile End Road; f.motallebi@qmul.ac.uk.

tunnel floor was flexible and the growth of a boundary layer along the working section could be controlled by adjusting the streamwise pressure gradient. The nominal air speeds at the tunnel throat were 10, 20, 30, and 40 m/s. Forward-wedge, counter-rotating joined V-shaped, and spaced counter-rotating vanes were investigated. Their results showed that SBVG devices with the heights on the order of only one-quarter of the boundary-layer thickness can significantly reduce the size of the separated region. Recently, Holden and Babinsky [16] carried out tests in a blowdown supersonic wind tunnel at the University of Cambridge using an array of wedge-shaped counter-rotating vanes at flow Mach numbers of 1.3 and 1.5 with a freestream Reynolds number of 28×10^6/m. The experiments showed that at a flow Mach number of 1.5, the vane-type vortex generators can generate stronger vortices closer to the surface and therefore are more effective than the wedge-type VGs at eliminating the boundary-layer separation. However, with these vortex generators, they observed the formation of extra shock waves at the leading and trailing edges of the vortex generators, which resulted in the formation of strong expansion waves over these devices. This extra shock waves cause an extra loss in the total pressure and hence higher wave drag. Popup sub-boundary-layer vortex generators have been used as flow controllers in many applications [17]. As an example, the SBVGs with a semicircular cross section and a height of 65% or less of the boundary-layer thickness have been introduced by Kuethe [18] and Rao and Kariya [19], the wire vortex generator was introduced by Ashil and Riddle [20], the circular and triangular forms of vortex generators have been introduced by Manor et al. [21], and the spanwise cylinders have been mounted horizontally at NASA by Dolling et al. [22]. Those investigations showed that popup devices are generally not successful for the purpose of separation removal with low excess drag.

A review of different separation control devices [23] showed that a low-profile vortex generator and passive cavity are both capable of reducing separation. A vortex generator is more applicable for a supersonic diffuser, because it causes more subsonic pressure recovery, and a passive cavity is probably more applicable for an airfoil, because it produces less wave drag. These investigations showed that to minimize the parasitic drag, low-profile vortex generators are considerably more effective.

In the present work, the performance of a new type of SBVG is presented: namely, the tetrahedral vortex generator (TVG).

II. Experiment Setup

A. Experimental Facilities

Experiments were carried out in a supersonic wind tunnel in the Whitehead high-speed laboratory at Queen Mary, University of London. The wind tunnel was an induction type that can provide a nominal freestream Mach number of 1.4 upstream of the shock location. The dry air, which was stored in a pressure vessel, provided a useful running time of about 60 s. The Reynolds number per unit length was about 16×10^6. The stagnation pressure and temperature were almost equal to the atmospheric values.

The location of the shock wave was controlled by a second chocking mechanism located downstream of the working section. Figure 1 shows the wind-tunnel dimensions. The working section of the wind tunnel had a length of 1220 mm with a uniform width of 126 mm. The height of the wind tunnel was 185 mm at the entrance, changing to 120 mm at the throat, with a gradual expansion to 150 mm at the exit. The observation windows were located 400 mm from the entrance. The second chock mechanism (which was used to adjust the location of the shock wave) was placed at 100 mm before the exit of the nozzle. The vortex generator was located at 280 mm downstream of the first row of pressure tapping. The position of the shock wave was kept constant at 130 mm downstream of the trailing edge of the TVGs. A roughness strip (1 mm thick and 2.5 mm wide) was placed immediately downstream of the first throat for the tripping of the boundary layer. The test section consisted of an instrumented aluminum flat plate. The plate was aligned with the plane of the upstream bottom wall of the wind tunnel. The surface of the plate was smooth and instrumented with 50 pairs of pressure tappings for the monitoring of the static pressure distribution and plugs for the insertion of the boundary-layer probe assembly.

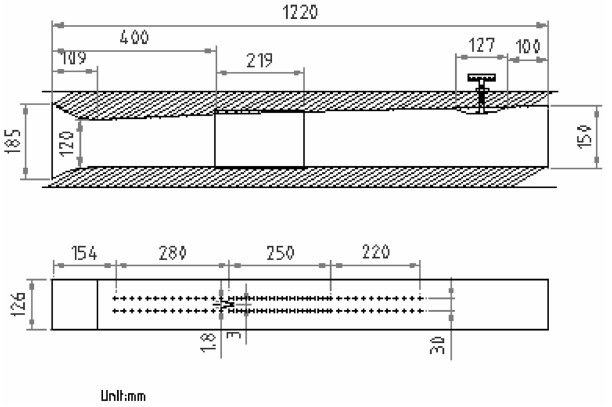

Fig. 1 Test section of the wind tunnel.

B. Measurements and Uncertainties

In the current experimental work, the performance of two sets of TVGs was investigated. The measurements consisted of streamwise measurements of wall static pressure, Preston pressure, and boundary-layer total pressure profiles and spanwise measurement of the total pressure profiles within the boundary layer.

For the measurement of the boundary-layer total pressure profiles, a flat-ended pitot tube was used. The flat pitot-tube tip allows correct boundary-layer measurement in a thin region close to the wall, with a higher resolution. A Digiplan stepper motor was used to traverse the boundary-layer pitot tube, which is supported by a data acquisition and processing program. In addition, a series of Preston probes with a 0.5 mm tip diameter were used to take measurements at smaller streamwise intervals. All pressures were recorded using a Scanivalve digital pressure transducer array that had a measurement accuracy of 0.5%. The standard deviation of 10 set of pressure records was always less than 0.06%. A computer-controlled Digiplan stepper motor was used to traverse the boundary-layer probe. The accuracy of the movement of the stepper motor was better than ± 0.075 mm, which is less than of 1% of the undisturbed boundary-layer physical thickness upstream of the interaction zone.

C. Model

The innovated model of the TVG used in the present work is the modified version of DERA's proposed flat-vane model [15], which has a tetrahedron geometry (Fig. 2). Two configurations of the model were examined and compared with the baseline. In both configurations, the distance between the trailing edge of the TVGs and the location of the shock wave was kept at 130 mm. At this distance, the thickness of the baseline boundary layer was 7.6 mm.

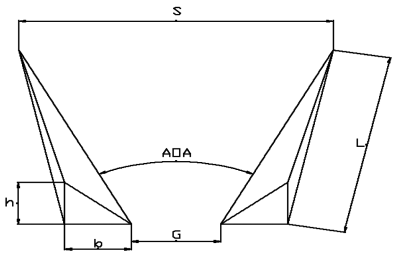

Model	L, mm	h, mm	b, mm	S, mm	G, mm
0.4δ	30	3	3	18	0
0.7δ	30	5	3	18	3

* AOA stands for Angle Of Attack which is dependent to S and G.

Fig. 2 Tetrahedral vortex generator.

III. Results and Discussion

A. Static Pressure

Figure 3 shows the streamwise distribution of the wall static pressure along the centerline of the wind-tunnel centerline for the two SBGVs configurations ($h = 0.7\delta$ and 0.4δ) as compared with the baseline case. Figure 3 clearly shows an increase in the static pressure around the location of shock wave (i.e., $x/\delta_R = 0$) for all cases. In all configurations, the flow starts with an almost-zero pressure gradient, followed by a relatively sharp increase in static pressure, which is then followed by a rather gradual increase further downstream of the shock wave. At point $x/\delta_R = 4.02$, the difference between the pressure ratio of the preceding arrangements is about 0.0319, and at point $x/\delta_R = 44.2$, it decreases to 0.021, which is about a 34% reduction.

B. Preston Pressure

Figure 4 shows the Preston pressure distribution of both TVG configurations compared with the baseline. In the baseline condition, the Preston pressure distribution shows the presence of a separated region between $x/\delta_R = -2.0$ and $+10.0$. This finding agrees with the surface oil-flow visualization (Sec. III.D and III.E), which shows that the length of the separated region is around $11.8\delta_R$. Further downstream, a gradual increase in Preston pressure distribution is an indication of reattachment of the boundary layer and flow recovery. Figure 4 also shows that both configurations have eliminated the separation region. Close inspection of the Fig. 4 also reveals that in the case of the smaller TVG, the Preston pressure recovery is more efficient than the larger TVG, which is an indication of more efficient momentum exchange within the inner part of the boundary layer.

C. Velocity Profile

Figures 5–14 show the streamwise distribution of boundary-layer velocity profiles. The velocity profile at $x/\delta_R = -5.36$, upstream of the interaction location, shows that the inner part of the velocity profile of the thicker TVG is more or less the same as the one corresponding to the thinner TVG . The velocity profiles from $x/\delta_R = -1.34$ and all further locations presented here show that the

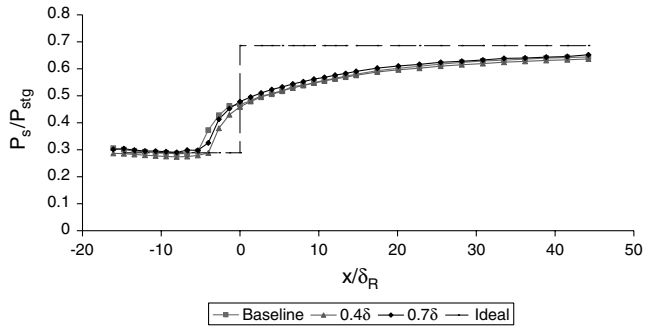

Fig. 3 Variation of the static pressure ratio along the tunnel for different height ratios.

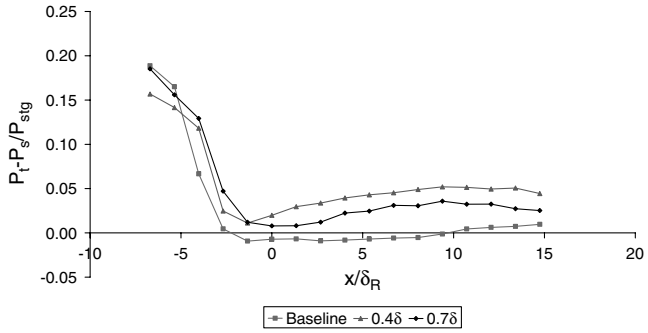

Fig. 4 Variation of Preston pressure along the tunnel for different height ratios.

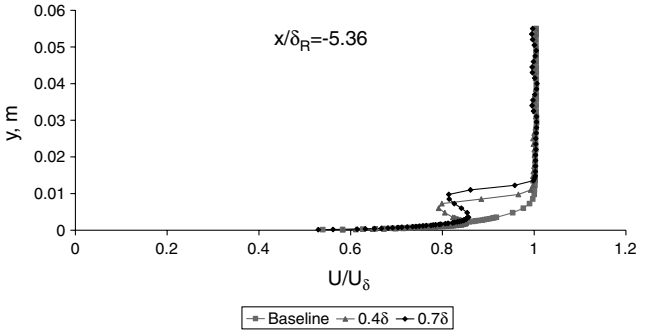

Fig. 5 Streamwise velocity profile for different height ratios at $x/\delta R = -5.36$.

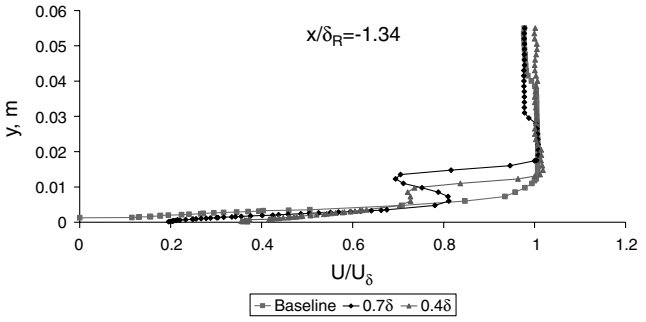

Fig. 6 Streamwise velocity profile for different height ratios at $x/\delta R = -1.34$.

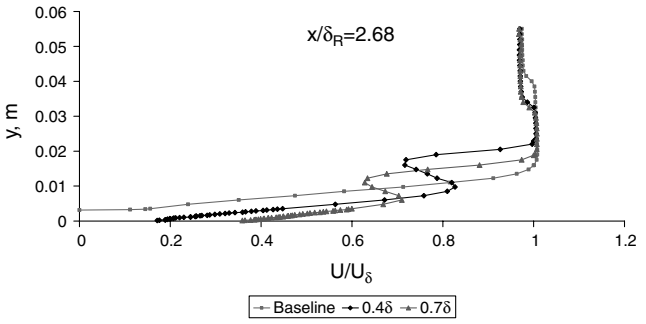

Fig. 7 Streamwise velocity profile for different height ratios at $x/\delta R = 2.68$.

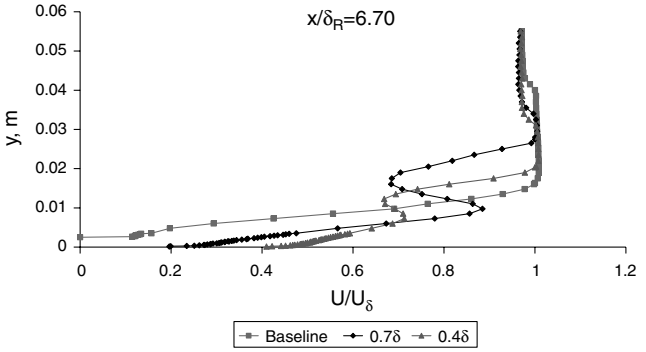

Fig. 8 Streamwise velocity profile for different height ratios at $x/\delta R = 6.70$.

velocity profile of the thicker TVG produces a less full profile near the surface as compared with the thinner TVG (Figs. 5 and 6). These figures also show that the larger TVG produces larger distortion in the velocity profile in the outer region of the boundary layer, which is

an indication of less efficient mixing in the boundary layer. It is also interesting to note that the edge of the boundary in the baseline case is more extended as compared with the controlled cases. This extended zone is probably due to the separation of the boundary layer and the formation of the Lambda shock pattern, which leads to a region of smaller stagnation-pressure loss downstream of the Lambda shock. On the other hand, the reduction in the stagnation pressure is higher in the lower part of the boundary layer when there are no VGs.

Similar behavior in the velocity profiles for these two configurations of TVGs is evident in Figs. 7 and 8. The trends of velocity profiles with SBVGs are continued in the further locations, shown in Figs. 7 and 8 ($x/\delta_R = 2.68$ and 6.70). They show that the effect of the larger TVG near the wall is less but produces a stronger swirled velocity profile and greater boundary-layer thickness with a larger displacement thickness.

Further downstream [i.e., $x/\delta_R = 10.72$ and 14.75 (Figs. 9 and 10)], the flow distortion in the boundary layer decreases and this trend continues further downstream, as can be seen in Figs. 11–14.

D. Boundary-Layer Parameters

Figure 15 shows the effect of TVG height on the boundary-layer thickness variation. The larger TVG clearly shows a thicker boundary-layer thickness in all locations, which as indicated earlier, is the result of the less efficient mixing within the boundary layer.

The streamwise distribution of the boundary-layer integral thicknesses are shown in Figs. 16 and 17. The larger TVG clearly produces higher displacement thickness throughout, which is an indication of less uniformity within the boundary-layer flow. As the flow approaches downstream, the two distributions approach each other, as expected. Figure 17 shows the streamwise variation of the boundary-layer momentum thickness. It is clear from Fig. 17 that the smaller TVG produces less momentum thickness and hence less losses than with the larger TVG.

The preceding observations indicate that although the boundary-layer parameters merge to more or less the same level for both devices, and both successfully eliminate separation, the thinner TVG is more efficient in the mixing process near the surface, with an obviously lower parasitic drag.

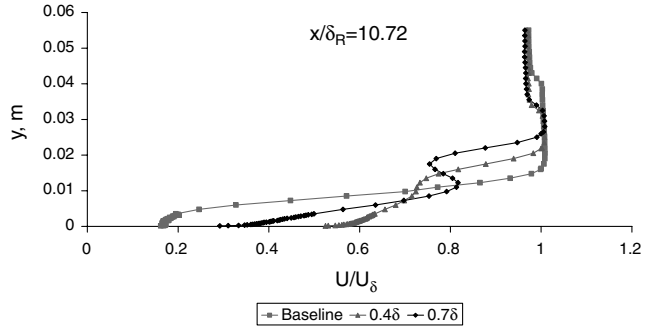

Fig. 9 Streamwise velocity profile for different height ratios at $x/\delta R = 10.72$.

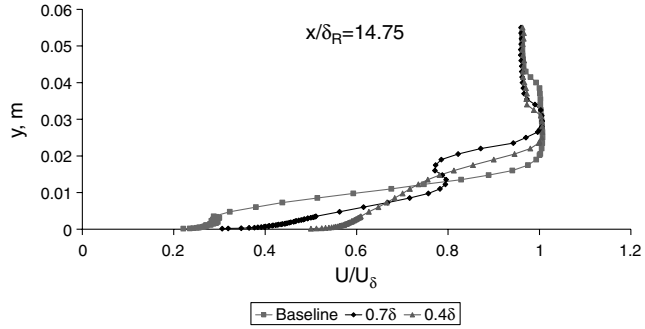

Fig. 10 Streamwise velocity profile for different height ratios at $x/\delta R = 14.75$.

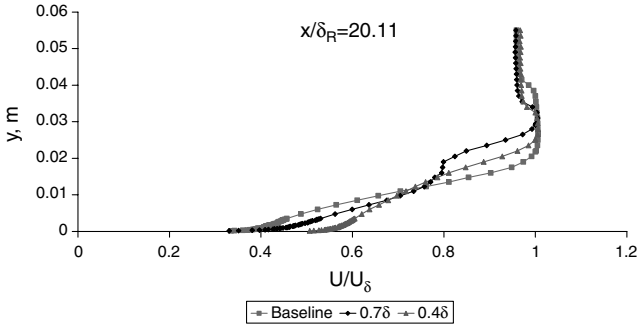

Fig. 11 Streamwise velocity profile for different height ratios at $x/\delta R = 20.11$.

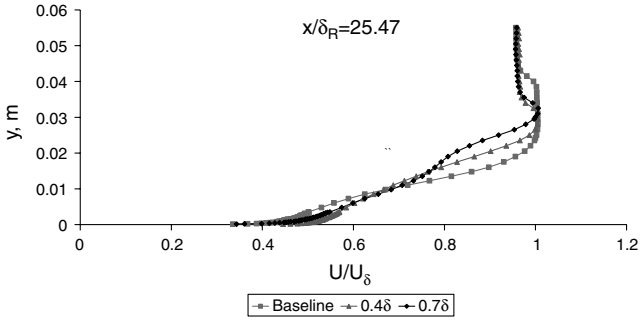

Fig. 12 Streamwise velocity profile for different height ratios at $x/\delta R = 25.47$.

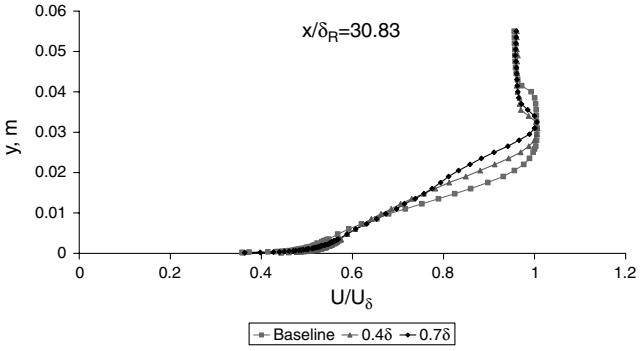

Fig. 13 Streamwise velocity profile for different height ratios at $x/\delta R = 30.83$.

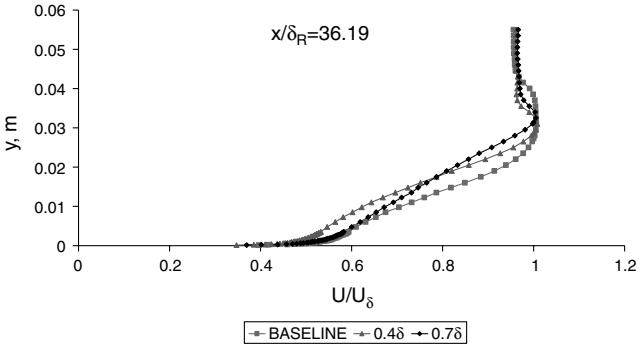

Fig. 14 Streamwise velocity profile for different height ratios at $x/\delta R = 36.19$.

Figure 18 shows the shape factor of both devices. The thicker VG, 0.7δ, shows an evolution of shape factor just upstream of the shock wave location. This is mostly the effect of low momentum thickness at this point. The shape factor of 0.4δ is more uniform than 0.7δ, a

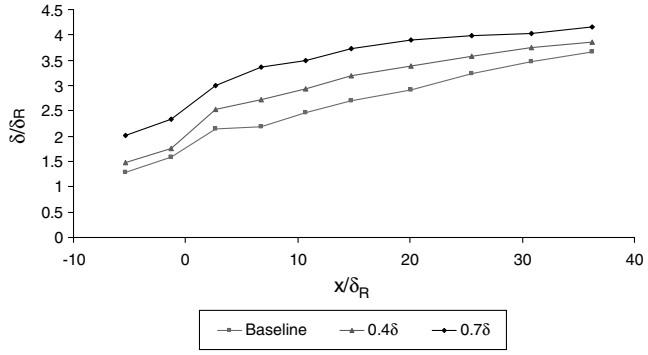

Fig. 15 Streamwise boundary-layer thickness for different height ratios.

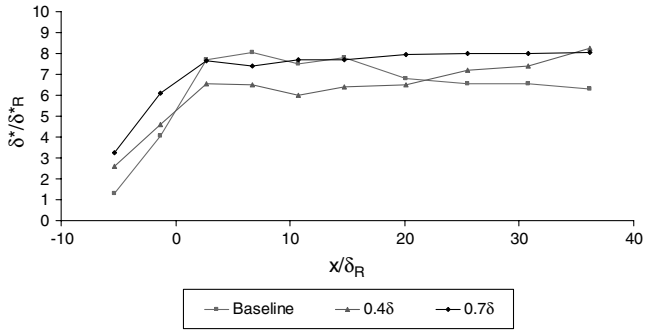

Fig. 16 Streamwise displacement thickness for different height ratios.

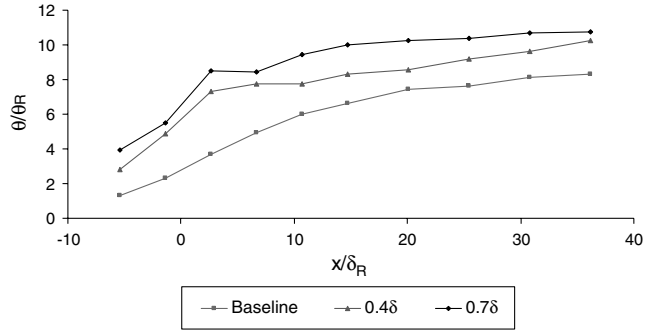

Fig. 17 Streamwise momentum thickness for different height ratios.

healthier shape factor. The shape factor of the controlled boundary layer is significantly different with the shape factor of baseline. The higher shape factor means a stronger adverse gradient. The hump in baseline shape factor represents the separation zone with high displacement thickness, and the worst point is located just after the shock location. The zone is associated with a high local pressure and a reverse flow. It displays the boundary layer sharply, and therefore the shape factor in the separation zone is high. A higher shape factor illustrates a shallow boundary layer.

The preceding observations indicate that although the boundary-layer parameters merge to more or less the same level for both devices, and both successfully eliminate separation, the thinner TVG is more efficient in the mixing process near the surface at a lower parasitic drag.

E. Surface Oil-Flow Visualization

Surface visualization is applied to observe the formation of flow on the surface. A mixture of titanium dioxide, oil, and oleic acid is used to visualize the flow over the surface and to observe the extent of shock-induced separation.

Figures 18a–18c show the surface flow-visualization topology for three cases in the separation region. In the baseline picture (Fig. 18a), the formation of separation in all spanwise areas is observable. Two large vortical structures are indicated where two spiral nodes at two sides reveal the domination of vortical structures. It is the evidence of the formation of reversed flow in the centerline region. The center of each vortical structure is about 25 mm from the sidewalls of the wind tunnel. The vortical structure of separation was developed symmetrically, and at the midspan region, there is a region of quasi-two-dimensional flow. The midspan length of this quasi-two-dimensional flow is about 15 mm. In the current work, the influence of vortex generators will be investigated in this quasi-two-dimensional flow around the centerline. The dynamic visualization of flow displayed the reverse flow in the midspan. The location of the separation line corresponded well with the location of the front leg of the Lambda shock structure, which is also about the point of sudden rise in static pressure. The reattachment point in the midspan is located at about a 90 mm distance from separation, which corresponds to a separation length of about $11.8\delta_R$.

Figures 18b and 18c shows that for both TVGs, the separation in the midspan region has completely disappeared as a result of the TVGs. The vena contracta thickness of the flow at the area of vanished separation is in the range of 15–18 mm for a 0.4δ height ratio and is slightly lower for a 0.7δ height ratio, and the leading gap of the pair of vortex generators is 18 mm. The small accumulation of oil just upstream of separation area is probably the result of the interaction of side vortical flows.

F. Spanwise Boundary-Layer Parameters

Traverse total pressure distributions at 7 spanwise points along the tunnel are investigated. The thinner VG, which showed a better performance in comparison with the other configuration, was verified and compared with the baseline. A rake system is served to detect spanwise traverse total pressure. For the baseline measurement, the results of P4 ($x/\delta_R = -1.34$) are shown. This is the shock wave location.

The spanwise boundary-layer thickness in baseline is almost constant; however, in the disturbed flow condition, spanwise boundary-layer parameters change drastically. In the portion close to the shock location, a considerable change in spanwise boundary-layer thickness can be observed. Figure 19 shows the spanwise boundary-layer thickness at points P3, P4, P5, P6, and P7, which correspond to $x/\delta_R = -5.36$, -1.34, 2.68, 6.70, and 10.72. Figure 20 shows that at point P3, changes in the flow regime affected the boundary-layer thickness, and the most effect occurred at the zone of the shock wave location represented at point P4. This effect is reduced at P5, and more reduction occurred at P6. In fact, the influence of the vortex generator here is weak. At P7, $x/\delta_R = 10.72$, there is not a considerable change in spanwise boundary-layer thickness, indicating that vortex generator influence vanishes. In all points, the boundary-layer thicknesses are greater than the baseline. Spanwise boundary-layer thickness for disturbed flow is almost symmetric, except at a pair of points around the centerline. This is most likely due to the unsymmetrical vortex generator arrangement. As expected, the boundary-layer thickness in further downstream sections becomes more stable and reaches a constant value in the spanwise direction.

Figure 21 shows spanwise absolute displacement thickness for five chosen streamwise points. Displacement thickness at the centerline and at two adjacent symmetrical spanwise distances from the center ($z = 6$ and -6) is almost constant for all measured streamwise points (P3–P7). Beyond this midspan to the next two symmetrical spanwise points ($z = 12$ and -12), a significant evolution of displacement thickness can be observed at point P4, which is the shock wave location. The evolution is observable at location P5 and then retarded in the two further downstream locations (P6 and P7), where the displacement thickness decreased. At further spanwise locations ($z = 18$ and -18), the rate of the displacement thickness is decreased. These observations suggest that the effect of the vortex generator for the attenuation or elimination of

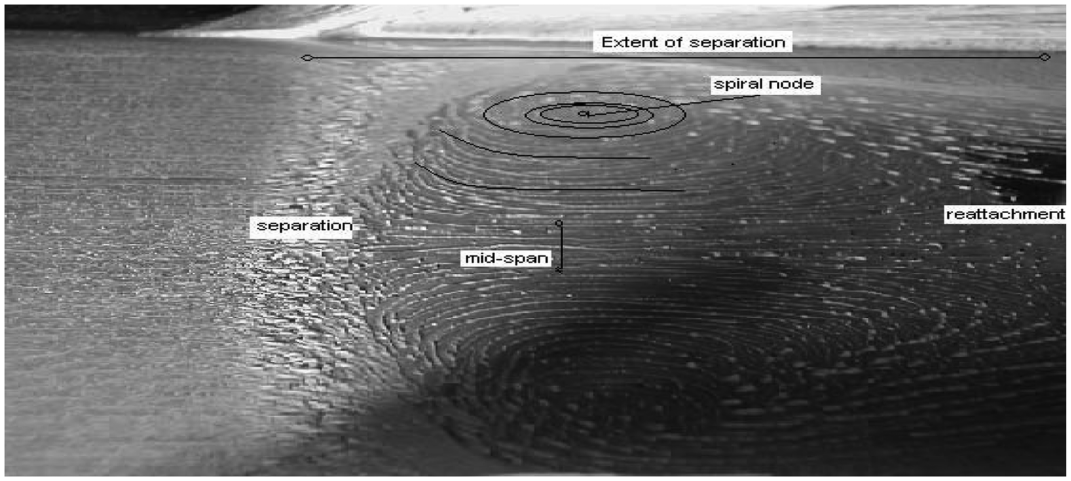

a)

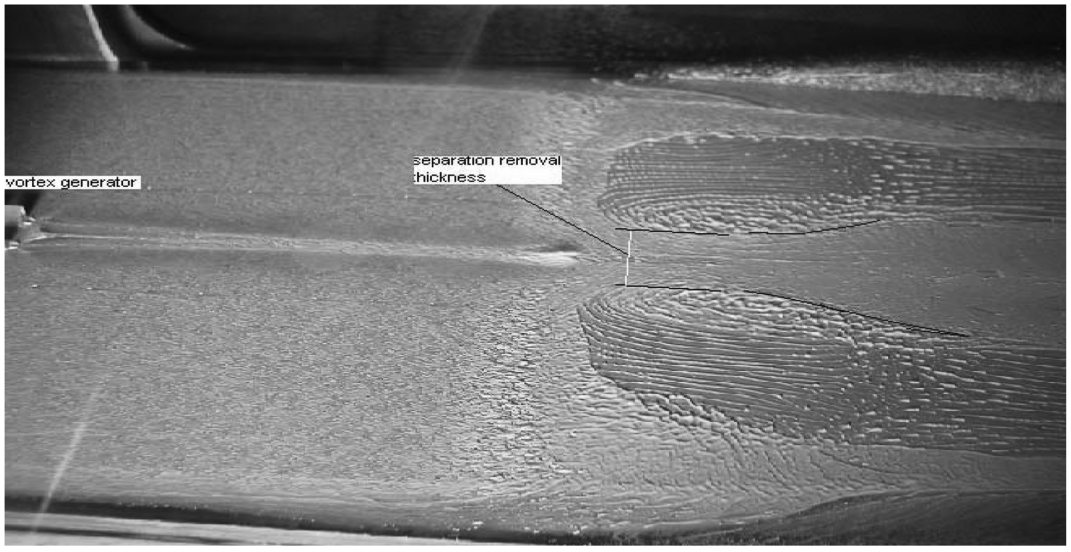

b)

c)

Fig. 18 Visualization of separation: a) baseline, b) 0.4δ, and c) 0.7δ.

separation occurs in the spanwise range of 12–24 mm, just downstream of the shock location. Referring to the oil visualization, the elimination of separation just downstream of the shock location is about 18 mm in the spanwise direction. Reduction of displacement thickness in these locations also dictates an approach to fully developed velocity profile downstream of location P5. Because the boundary-layer displacement is affected by boundary-layer thickness and velocity profile, from downstream of P5, the velocity profile performance dominates the effect of boundary-layer thickness. The most uniform displacement thickness appears in the last location (P7), which shows that the effect of vortex generator is reducing.

At point P3, upstream of the shock location, the displacement thickness is lower than downstream in all spanwise measured points, as the flow is only slightly affected by the shock wave and its induced

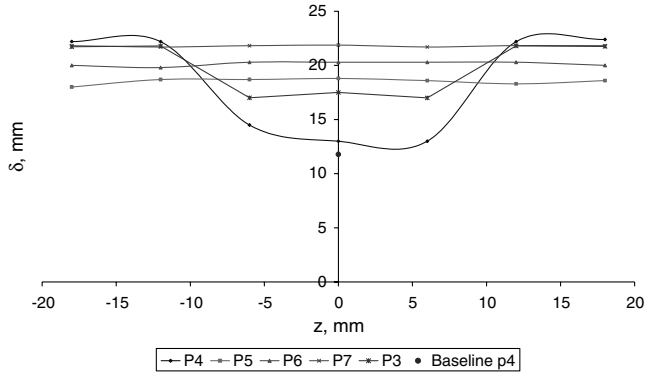

Fig. 19 Spanwise absolute boundary-layer thickness of the VG at points P3, P4, P5, P6, and P7, representing, correspondingly, $x/\delta R = -5.36, -1.34, 2.68, 6.70$, and 10.72.

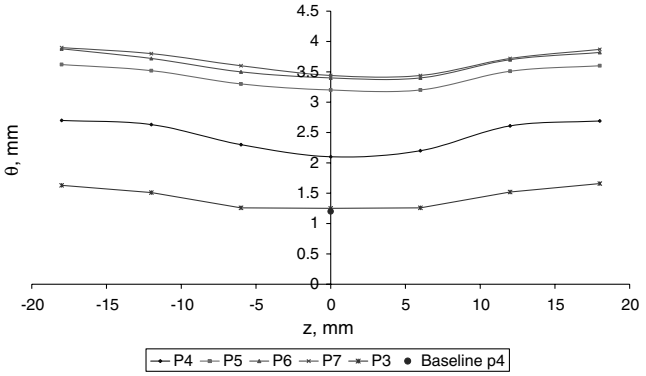

Fig. 21 Spanwise absolute momentum thickness for P3, P4, P5, P6, and P7, representing, correspondingly, $x/\delta_R = -5.36, -1.34, 2.68, 6.70$, and 10.72.

effect on the boundary layer. In the points beyond the midspan, the slight evolution on displacement thickness is the backward-interference effect of the shock/boundary interaction. Baseline displacement thickness at point P4 is about 4 mm and is less than the displacement thickness at the same location with the vortex generator. Figure 21 also illustrates slightly unsymmetrical curves of displacement thicknesses, which is probably the result of unsymmetric development of counter-rotating vortices produced by the slightly unsymmetrical arrangement of the pair of vortex generators.

Spanwise momentum thickness of the disturbed boundary layer in some streamwise locations is shown in Fig. 21. In the midspan location ($z = -6$ to 6), the momentum thicknesses at P4 (and also P5, P6, and P7) is almost uniform. Beyond this spanwise range at P4, an evolution in momentum thickness occurs so that at the points $z = 12$ and -12, the momentum thickness has risen about 25% above the centerline. Beyond these points and at the points $z = 18$ and -18, the momentum thickness rises further, but with a lower rate. This shows that the elimination of separation in the spanwise direction is effective in the range of 12–24 mm spanwise at about the shock wave location. The spanwise effect is extended in further downstream locations. It is already established that the effective elimination of separation with the vortex generator is about 18 mm spanwise at just the shock location. Figure 18 also illustrates slight unsymmetrical curves of momentum thicknesses, which is mostly the effect of the unsymmetrical arrangement of the pair of vortex generators.

The spanwise shape factor for the disturbed boundary layer is shown in Fig. 22. This figure shows that at P4, the shape factor in the centerline zone is low and an evolution appears at and beyond the points $z = 12$ mm and -12. This is due to high displacement thickness at these points, as shown in Fig. 21. In the further downstream sections, the shape factor approaches a uniform quantity, due to attenuation of the vortex generator effect. A comparison between

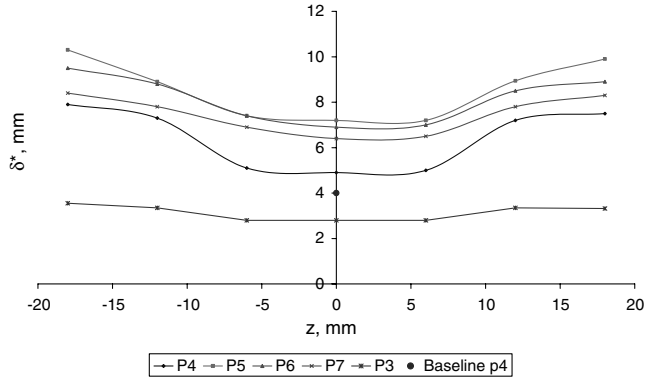

Fig. 20 Spanwise absolute displacement thickness for P3, P4, P5, P6, and P7, representing, correspondingly, $x/\delta R = -5.36, -1.34, 2.68, 6.70$, and 10.72.

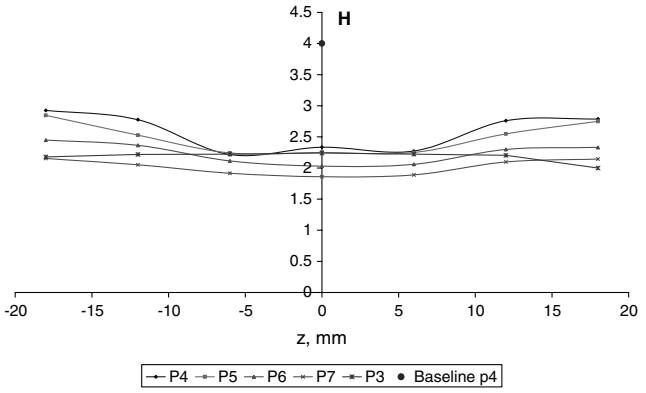

Fig. 22 Spanwise shape factor for P3, P4, P5, P6, and P7, representing, correspondingly, $x/\delta_R = -5.36, -1.34, 2.68, 6.70$, and 10.72.

the baseline shape factor and the disturbed shape factor from P4 to the downstream points clearly shows that the baseline shape factor is much higher than the disturbed shape factor. This indicates that in a disturbed flow, although the effective spanwise range of elimination of separation is as low as 18 mm, the effect propagates beyond this range. This effect is associated with a higher momentum thickness than the baseline. The higher momentum thickness causes a lower shape factor.

IV. Conclusions

In the current work, the performances of two submerged vortex generators are examined: the vortex generator with height ratios of 40% of the boundary-layer thickness (0.4δ) and 79% (0.7δ). Both are pairs of vortex generators with 30 mm length, 3 mm base, 18 mm leading gap, 3 mm trailing gap placed 130 mm upstream of shock wave, and thicknesses of 0.4δ and 0.7δ, respectively. It is expected that an increase in the thickness of the SBVG will increase the mixing process, but at the expense of a higher parasitic drag.

The results show that TVGs are capable of producing vortices without a considerable parasitic boundary layer. They could totally eliminate the shock-wave/boundary-layer separation. But changing the height ratio from 0.4δ to 0.7δ did not produce a better performance in terms of controlling the shock-induced separation. These results confirm that a thicker vortex generator produces more displacement thickness at the expense of a thicker boundary layer and a lower surface total pressure.

References

[1] Wheeler, G. O., "Means for Maintaining Attached Flow of a Flowing Medium," U.S. Patent No. 4455045, 19 June 1984.

[2] Farokhi, S., and Taghavi, R. R., "Supersonic Vortex Generator," U.S. Patent No. 5598990, Feb. 1997.

[3] Farokhi, S., *Propulsion System Design with Smart Vortex Generators*, Pergamon, New York, 1998.
[4] Delery, J. M., "Shock Phenomena in High Speed Aerodynamics: Still a Source of Major Concern," *The Aeronautical Journal*, Vol. 103, No. 1019, Jan. 1999, pp. 19–34.
[5] McCormick, D. C., "Shock-Boundary Layer Interaction Control with Low-Profile Vortex Generators and Passive Cavity," *30th Aerospace Meeting and Exhibit*, AIAA, Washington, D.C., Jan. 1992, pp. 2–9.
[6] Bur, R., and Corbel, B., "Experimental Study of Transonic Interaction with Shock and Boundary-Layer Control," *Fluid 2000*, AIAA, Reston, VA, 2000, pp. 1–11.
[7] Smith, A. N., Babinsky, H., Fulker, J. L., and Ashill, P. A., "Control of Normal Shock Wave/Turbulent Boundary-Layer Interaction Using Streamwise Slots," 39th Aerospace Science Meeting and Exhibit, Reno, NV, AIAA Paper 2001-0739, 2001.
[8] Wheeler, G., "Low Drag Vortex Generators," U.S. Patent No. 5,058,837, 22 Oct. 1991.
[9] Donaldson, C., "Investigation of a Simple Device for Preventing Separation Due to Shock and Boundary-Layer Interaction," NACA RM L5OB02a, 1950.
[10] Edwards, J. B. W., "Free-Flight Tests of Vortex Generator Configurations at Transonic Speeds," Royal Aircraft Establishment, TN Aero 2862, London, Dec. 1962.
[11] Westkaemper, J. C., and Whitten, J. W., "Drag of Vane-Type Vortex Generators in Compressible Flow," *Journal of Spacecraft and Rockets*, Vol. 7, No. 10, 1970, 1269–1271.
[12] Lin, J. C., "Application of Micro-Vortex Generators for Turbulent Flow Separation Control," NASA Langley Research Center, Hampton, VA.
[13] Lin, J. C., Robinson, S. K., and McGhee, R. J., "Separation Control on High-Lift Airfoils via Micro-Vortex Generators," *Journal of Aircraft*, Vol. 31, No. 6, Nov.–Dec. 1994, pp. 1317–1323. doi:10.2514/3.46653
[14] Lin, J. C., Howard, F. G., and Selby, G. V., "Small Submerged Vortex Generators for Turbulent Flow Separation Control," *Journal of Spacecraft and Rockets*, Vol. 27, No. 5, Sept.–Oct. 1990, pp. 503–507. doi:10.2514/3.26172
[15] Ashill, P. R., Fulker, J. L., and Hackett, K. C., "Research at DERA on Sub Boundary Layer Vortex Generators," Defence Evaluation and Research Agency, Aerodynamic Dept., Bedford, England, U.K., 1999.
[16] Holden, H. A., and Babinsky, H., "Vortex Generators Near Shock/Boundary Layer Interactions," AIAA Paper 1242, 2004.
[17] Motallebi, F., "Flow Control," Queen Mary, Univ. of London, London, 2003.
[18] Kuethe, A. M., "Boundary Layer Control of Flow Separation and Heat Exchange," U.S. Patent No. 3741285, issued 26 June 1973.
[19] Rao, D. M., and Kariya, T. T., "Boundary Layer Submerged Vortex Generators for Separation Control—An Exploratory Study," AIAA Paper 1988-3546, 1988.
[20] Ashil, P. R., and Riddle, G. L., "Sub Boundary Layer Vortex Generators," International Patent Classification Published Under the Patent Cooperation Treaty (PCT), B64C 21/10, 23/06, 1995.
[21] Manor, D., Dima, C., Schoch, P., and Polo, J., "Using Popup Vortex Generators on the Wing Surface to Greatly Increase the Lift and Stall Angle of Attack," AIAA Paper 1993-1016, 1993.
[22] Dolling, D. S., Fourier, E., and Shau, Y. R., "Effect of Vortex Generators on the Growth of a Compressible Shear Layer," *Journal of Propulsion and Power*, Vol. 8, No. 5, Sept.–Oct. 1992, pp. 1049–1056. doi:10.2514/3.23591
[23] Lin, J. C., "Review of Research on Low-Profile Vortex Generators to Control Boundary Layer Separation," *Progress in Aerospace Sciences*, Vol. 38, Nos. 4-5, 2002, pp. 389–420. doi:10.1016/S0376-0421(02)00010-6